

Shock Excitation in Interacting Galaxies: Mkn 266

R. Davies

Max-Planck-Institut für extraterrestrische Physik, Postfach 1603, 85470 Garching, Germany

M. Ward

Department of Physics & Astronomy, University of Leicester, University Road, Leicester,
LE1 7RH, UK

and

H. Sugai

Department of Astronomy, Kyoto University, Sakyo-ku, Kyoto 606-8502, Japan

ABSTRACT

We present near infrared data on the luminous interacting system Mkn 266 (NGC 5256), comprising $2\mu\text{m}$ continuum, and $\text{Br}\gamma$ and 1-0 S(1) emission line images, together with K-band spectra. We have fitted stellar templates to the continuum, allowing us to account for all the stellar features and hence detect even faint gas excitation emission lines, including 8 and 11 H_2 lines in the SW and NE nuclei respectively. Population diagrams for the excited H_2 molecules indicate that most of the 1-0 S(1) in each of the nuclei has a thermal origin. We discuss this with reference to the observed morphologies, especially that of the 1-0 S(1) line. In particular, the core of 1-0 S(1) in the NE nucleus is more compact than the $2\mu\text{m}$ continuum; while in the SW nucleus the 1-0 S(1) is significantly offset by 500 pc from the continuum (and other) emission. Lastly we address the issue of the region midway between the two nuclei, where previously a strong source of radio continuum has been observed. These results are set in the context of interacting galaxies where shock excited emission might be expected to occur as a direct consequence of the interaction.

Subject headings: galaxies: individual (Mkn 266) – galaxies: interactions – galaxies: nuclei – infrared: galaxies – line: formation

1. Introduction

Prompted by the discovery from CO observations that the bulk of the molecular gas in close mergers can quickly congregate between the nuclei (Gao et al. 1997, Scoville et al. 1997), we have begun to look at number of such systems, imaging the 1-0 S(1) and Br γ lines since the morphologies of these with respect to the continuum and each other can provide important information. The rationale is that while star formation models allow a quantitative analysis of the observed fluxes, the results can be quite misleading if the distribution of the emitting regions is not considered. Compare, for example, an object in which the Br γ and 2 μ m continuum come from the same region (in which a single burst of star formation is possible), to one in which they are offset from each other, *requiring* two distinct epochs of activity. A classic example is given by González Delgado et al. (1997) who found both Wolf-Rayet and CaII features in the super star cluster A of NGC 1569, implying the simultaneous presence of hot massive stars and red supergiants. Their interpretation required the existence of non-coeval stellar populations in the same stellar cluster. The difficulty was resolved when De Marchi et al. (1997) found from HST imaging that this was actually 2 distinct clusters. Such high resolution is not always required, and in a small sample of blue compact dwarf galaxies observed by Davies et al. (1998), the Br γ , 1-0 S(1), and 2 μ m continuum all had strikingly different morphologies on scales of a few arcsec (\sim 100 pc). In such cases a simple interpretation of the emission in terms of just star formation is not valid.

Another issue which has posed a significant barrier to extragalactic work is the detection of the fainter H $_2$ lines, which is essential to determine the fractions of H $_2$ which are thermally and non-thermally excited. Previously, except in a few cases such as NGC 6240 (Sugai et al. 1997b) which has extremely bright 1-0 S(1), this has typically relied on very few line ratios, often given only as upper limits and extracted from rather large apertures (eg Goldader et al. 1997). It is crucial to detect lines from the v=2 (or higher) bands: a single thermal model can nearly always provide a reasonable fit to lines from the v=1-0 transitions. It is also important to have more than one v=2-1 line, since ratios involving only a single such transition can be ambiguous: for temperatures in the range 1500–2500 K, the thermal 2-1 S(1)/1-0 S(1) ratio varies from 0.03 to 0.15. Thus if a ratio (or upper limit) of 0.15 is observed, while the 1-0 S(1) is constrained to be $>$ 75% thermal, the *total* H $_2$ cooling can only be attributed to somewhere in the range 35–100% thermal depending solely on a fairly small change in thermal excitation temperature. With the increasing sensitivity of near-infrared detectors it is now possible to use small apertures and obtain the high signal-to-noise spectra required to detect higher vibrational lines. Additionally, fitting the continuum with stellar templates, rather than using a power-law or polynomial fit, is necessary in order to take account of the stellar features and allow weak lines from the excited gas, such as H $_2$ lines, to be measured reliably.

We address these issues in this paper, in which we present a detailed analysis of near infrared emission line images and spectra. We focus on Mkn 266, a luminous infrared galaxy ($L_{\text{IR}} = 3 \times 10^{11} L_{\odot}$) at a distance of 115 Mpc ($1'' = 560$ pc). It has 2 prominent nuclei $10''$ apart, with a common envelope, suggestive of a merger (Mazarella et al. 1988, hereafter MGAH). There

have been very few detailed studies of Mkn 266, the two most decisive being those of MGAH and Wang et al (1997). The former authors presented an H α map which revealed arcs that may be tidal tails or remnant spiral structure. They also mapped the radio continuum, which appears similar to the 2 μ m continuum but with a strong region of extended emission halfway between the nuclei. The latter study found evidence for a superwind in their X-ray imaging and spectroscopic data.

2. Observations and Data Reduction

2.1. Fabry-Perot Images

Images of the 2 μ m continuum, and 1-0S(1) and Br γ emission lines were obtained with the UKIRT 3.8-m telescope on Mauna Kea, on the nights of 12 and 13 May 1998. A K-band Fabry-Perot etalon (FP), set in a collimated beam, was used in conjunction with IRCAM3 (a 256 \times 256 InSb array) at the Cassegrain focus. The scale of 0.286'' per pixel gave an unvignetted field of view of $\sim 60''$. Order sorting was achieved with cooled narrow band filters: 2.4% FWHM for the Br γ line, and 4.25% FWHM for the 1-0S(1) line. The latter filter is normally used for continuum imaging, but was required due to the large recession velocity ($> 8000 \text{ km s}^{-1}$) of the galaxy which shifted the line out of the standard filter pass-bands. The 325 km s^{-1} spectral resolution of the FP and the wavelength calibration were checked several times during the night using the 2.1171 μ m line from a Krypton lamp, permitting adjustments for temperature changes (approx. 40 $\text{km s}^{-1}/^\circ\text{C}$).

Due to the relatively small size of Mkn 266 we imaged it at 2 positions on the detector, symmetrically off-axis from the centre of the FP (14'' North-West and 14'' South-East). The transmitted wavelength varies off-axis as $\delta\lambda \propto r^2$, reaching $\delta\lambda \equiv 160 \text{ km s}^{-1}$ at $r = 30''$, hence the difference is only $\delta\lambda = 40 \text{ km s}^{-1}$ at $r = 14''$. This was taken into account when setting the FP wavelength. Other concerns include the small 15 km s^{-1} offset for the velocity of the earth relative to the sun in the direction of the object on that date, which was not included, and the uncertainty in the heliocentric line velocity. Our adopted value was 8385 km s^{-1} , the average for the two nuclei determined from optical spectra by Veilleux et al. (1995), resulting in additional offsets of $\pm 25 \text{ km s}^{-1}$ for each nucleus. Although each of these adjustments is small, they must all be considered: with a FWHM resolution for the FP of 325 km s^{-1} , a total offset of 100 km s^{-1} will mean that the line flux is underestimated by 35%, but a reduction to only 50 km s^{-1} (similar to the maximum we expect) results in a net effect on the line flux of less than 10%. A similar consideration applies to the line dispersion, which can reduce the line flux detected if it is much greater than 100 km s^{-1} . Typical corrections are 20% for 200 km s^{-1} , and 35% for 300 km s^{-1} , but it should be noted that they combine with velocity offsets non-linearly. Line dispersion effects were not included in the line flux estimation since the line-widths are not known, although they are expected to be relatively narrow for starbursts.

Observations were carried out in blocks, each of which had 4 integrations of 3 minutes per pointing, consisting of: 2 at the on-line wavelength, and one each for continuum at slightly shorter and longer wavelengths (shifted with respect to the line centre by -800 and $+1000 \text{ km s}^{-1}$ respectively). Standard A-type stars (BS 4344 and BS 5142) were observed between each set of 2 or 3 blocks. The total on-line integrations were 48 mins for $\text{Br}\gamma$, and 120 mins for 1-0 S(1).

IRAF was used for all image processing and analysis as described below. Flatfields were made using opposite positions after dark current subtraction. These consist of the camera flatfield, and a smooth circularly symmetric contribution from the FP. Due to small temperature variations, the latter changed slightly between successive integrations (at the 1% level), leaving a residual ripple. Although this makes little difference to the continuum counts, it is crucial to the detection of line flux since the *peak* line counts per pixel are only 2% of the sky background. Thus after each frame was dark subtracted and flatfielded, it was also divided by the median filtered combination of itself rotated every 22.5° about the centre of the ripple pattern. A constant value for the sky could then be subtracted (rather than using sky frames which would increase the noise). The frames were aligned on the NE nucleus since it is more compact than the SW one, but this could introduce systematic offsets due to the line emission in the on-line frames. In order to check that there was no such bias, the centroid positions between pairs of successive off-line and on-line images (at the same telescope pointing) were compared. For the $\text{Br}\gamma$ line these were $x = -0.17 \pm 0.47$ pixels and $y = 0.05 \pm 0.27$ pixels; for 1-0 S(1) they were $x = -0.10 \pm 0.12$ pixels and $y = 0.24 \pm 0.20$ pixels (1 pixel = $0.286''$). For both lines, the mean difference was less than the RMS variation and systematic effects should not be more than $\sim 0.1''$.

Flux calibration was achieved with the standard stars BS 4344 (type A4V, $K=6.30$) and BS 5142 (type A3V, $K=5.18$). The frames were treated in the same way except that sky frames were subtracted and there was no need to correct for the ripple pattern. The profiles of the order sorting filters were included, making as much as 15% difference from assuming a simple boxcar shape due to secondary FP transmission orders in the wings of the pass-band. The image resolution was determined from the stars to be $0.77''$ for the 1-0 S(1) line and $1.34''$ for the $\text{Br}\gamma$ line.

The continuum image was deconvolved with 30 iterations of the Lucy algorithm implemented in IRAF, after halving the pixel size. The iterations were stopped once false structure due to noise peaks began to show in the fainter emission. At this point the stronger emission peaks show only genuine features; for example, the asymmetry in the NE nucleus in the deconvolved image is also apparent (just) in the direct image. The resolution of $0.36''$ was determined by including at one edge of the image an extra region with the same noise and a number of Gaussians convolved with the PSF; after deconvolution, the recovered and original sizes were compared.

2.2. Longslit Spectroscopy

Spectra of Mkn 266 were obtained as part of the UKIRT service observing programme on May 1 1999 using the CGS4 spectrometer; the orientation of the slit, 33° East of North, is indicated on Fig. 1. The total integration time was 64 min. Frames are sky subtracted, flatfielded, and co-added on-line using CGS4DR; further data reduction was carried out with IRAF. The dispersion axis was aligned to pixel rows, and the spatial axis to pixel columns with reference to an argon arc lamp and hence simultaneously calibrating the wavelength scale. Standard A stars (BS 5023 and HD 105601) were used for flux calibration and atmospheric correction after interpolating over $\text{Br}\gamma$ and $\text{Pa}\alpha$ with Lorentzian profiles and making a small correction to the same airmass as Mkn 266. The spatial resolution was determined from the standard stars to be $1.06''$, well matched to 2-pixel sampling. Integrated spectra of each nucleus were extracted in order to look at weak features, and additionally the spatial extent of the brighter features was considered. The heliocentric velocities of the two nuclei were measured as 8440 km s^{-1} (NE) and 8390 km s^{-1} (SW), in good agreement with those of Veilleux et al. (1995).

3. Emission Line Images

The continuum image (upper left and, deconvolved, upper right) in Fig 1 shows that the 2 nuclei are separated by $10.5''$, 5.9 kpc at the distance of the galaxy. The NE nucleus is resolved with a size of $0.8'' \times 0.6''$. As Fig 2 shows the 1-0S(1) is more compact than this: comparison via quadrature correction with the continuum would put its size at $\lesssim 0.45''$. This is similar to the extent of the radio source observed at 6 cm by MGAH, which was marginally resolved at a resolution of $0.3'' \times 0.4''$, and found to have a spectral index of 0.61 ± 0.04 .

The continuum in the SW nucleus has a morphology very similar to the radio continuum: central source with extensions to $\sim 1''$ at position angles slightly west of North and east of South. The $\text{Br}\gamma$ may also include these regions but the poorer resolution rules out a definitive statement. Nevertheless, the presence of a fairly substantive continuum component argues against the suggestion of MGAH that these are radio jets from the Seyfert nucleus, and tends towards interpretation in terms of star formation. An interesting point is that the high CO index measured in the spectrum by Goldader et al. (1997), $\text{CO}_{\text{ph}} = 0.16 \pm 0.03$, suggests the presence of late-type supergiants, which would only be expected in a young stellar population. Such a conclusion is consistent with our spectra which suggest a 50% contribution from supergiants in the K-band, twice that of the NE nucleus. The implied spatial scales on the order of 1 kpc are consistent with what is known about circumnuclear star formation occurring at inner Lindblad resonances around an AGN/starburst. It should be noted, however, that there is currently no evidence for the barred potential in a disk which would lead to gas inflow to such resonances. Indeed, the $\text{H}\alpha$ and optical morphologies (MGAH) are highly perturbed.

The 1-0S(1) in this region emission is rather unexpected, the peak being offset from the

continuum by $0.9''$. As described in Section 2, although the images were aligned on the NE nucleus, systematic effects cannot account for these offsets. The 1-0S(1) line map has a higher signal-to-noise and good resolution, so we can be confident that the offset is real. For the Br γ map a big uncertainty lies in the low signal-to-noise (peak pixel in the smoothed image is 7.5σ), and the relatively poor resolution ($1.3''$). We therefore cannot claim any significance in the Br γ offset. Astrometry with the 6 cm radio map of MGAH suggests that the Br γ and $2\mu\text{m}$ continuum are aligned with the Seyfert nucleus.

4. Spectra

An integrated spectrum of each nucleus was extracted, covering 5 pixels ($3.05''$) along the slit by the slit width of $1.22''$, and these are shown in Fig. 3. Additionally, the spatial extent of some stronger features could be mapped, as shown in Fig. 6. Clearly the system is far from trivial, and it would be useful to analyse all the line ratios with high spatial resolution, something which may be possible with adaptive optics and integral field spectroscopy in the (near) future (eg see Davies et al. 1999). Here we present an analysis of the detailed integrated spectra together with some spatial information from both spectra and images.

4.1. Continuum Fitting & CO Absorption

In order to recover emission lines which are either faint or superimposed on absorption features it is important to subtract an accurate continuum rather than fit a simple line or curve as is often done. This has the double benefit of also providing a qualitative estimate of the stellar population contributing to the $2\mu\text{m}$ emission. We used a minimum chi-square fitting routine with the following restrictions:

- (1) only regions of the continuum distinct from emission lines were included in the chi-square estimations;
- (2) a single value for extinction was fitted;
- (3) a hot dust component (eg for an AGN) was not included as it did not improve the fits.

The CO absorption indicates that late-type giant & supergiant stars dominate the continuum at these wavelengths and so we used generic spectra of these types, created by adding several examples of each from the library of Förster-Schreiber (1999) and convolving them to the same resolution as our data. The individual templates have varying spectral coverages (dependent on the resolution), resulting in a trade-off between large coverage of $2.00\text{--}2.44\mu\text{m}$ or a wider variety of stellar types but covering only $2.27\text{--}2.40\mu\text{m}$. The latter range of templates includes M I, K I, K0 III, K5 III, M0 III, which cover the range of types required; adding any other available spectra (eg between K0 and K5 giants) would not provide any further useful information about the stellar population. The former range of types misses out the M0 III and, more seriously, K I. Nevertheless,

both approaches gave the same qualitative result, and so we used the former one in order to provide the longest possible baseline for subtraction. The stellar types used were M1, K0 III, and K5 III, and the best fits had RMS errors of ~ 0.06 per data-point (for the scales in Fig. 3). The baseline of the fitted continuum was extended down to $1.85\mu\text{m}$ by adding a much lower resolution spectrum of a late-type giant star, also reddened with the same extinction, from the PEGASE database (Fioc & Rocca-Volmerange 1997).

The result showed that about 20–25% of the $2\mu\text{m}$ continuum in the NE nucleus is from late-type supergiants, while the rest is from giants, and the extinction is $A_V \sim 3.2$ mag; in the SW nucleus about 50% is from supergiants, with $A_V \sim 4.6$ mag.

We have additionally tried to constrain the stellar population by measuring the CO index directly. We have used two indices, CO' of Goldader et al. (1997) in the $2.30\text{--}2.34\mu\text{m}$ interval, and CO_{sp} of Doyon et al. (1994) in the $2.31\text{--}2.40\mu\text{m}$ range. Converting these to CO_{ph} , using the relations given by Goldader et al., gives similar values for the two indices. These values are $CO_{\text{ph}} = 0.12$ (NE) and 0.16 (SW). The latter value verifies that there is a higher supergiant fraction in the SW nucleus, and is the same as that measured by Goldader et al. even though they used a much larger $3'' \times 9''$ aperture.

4.2. H₂ Excitation

The process described above removes much of the structure in the continuum, including such features as Mg ($2.14\mu\text{m}$), Na ($2.21\mu\text{m}$), Ca ($2.26\mu\text{m}$), etc. It allows not only weak lines to be measured, but also the Q-branch H₂ lines – which is useful since the 1-0 Q(3) and 1-0 S(1) lines come from the same upper level, as do 1-0 Q(2) and 1-0 S(0), providing a consistency check when plotting a population diagram for the molecules.

The H₂ line ratios relative to 1-0 S(1) in each nucleus are given in Table 2, and level population diagrams are shown in Figs. 4 and 5, which have been derived assuming the local thermal equilibrium ortho-para ratio of 3. This should be valid for thermally excited H₂, but it is generally found that for H₂ excited by UV fluorescence the ortho-para ratio is ~ 2 . Sternberg & Neufeld (1999) argue that this is because the ortho absorption lines become optically thick sooner than the para absorption lines, so UV pumping of the ortho states is less efficient and the ortho-para ratio appears to be reduced to a limiting case of $\sim \sqrt{3} = 1.7$. That is, the UV excited states (those observed) have an apparent ortho-para ratio of 1.7, while the total H₂ ratio remains at 3. This effect only occurs if the absorption lines become optically thick to UV pumping, and is included in the line strength calculations of Black & van Dishoeck (1987) from whom we take our models of UV fluorescence. However, for the purposes of fitting fluorescent models to the population diagram, the ortho-para ratio used does not actually matter as long as the same ratio is used for both the observed and modelled spectra when converting line strengths to level populations. For simplicity, therefore, since we do not know *a priori* the relative

thermal/non-thermal contributions (which is what determines the observed ortho-para ratio), we have adopted the same ratio as in the LTE case.

For one model, we have fitted a combination of thermal and non-thermal components, with the 3 free parameters being the relative non-thermal contribution f_{UV} to the 1-0 S(1) line, the temperature T of the thermal component, and the absolute scaling. For the non-thermal component we used fluorescent model 14 from Black & van Dishoeck (1987), although this could equally well be formation pumping which results in a similar spectrum. For the thermal component we used the Boltzmann distribution at temperature T given by

$$\frac{N_u}{g} \propto e^{-E_u/kT} \quad \text{with} \quad N_u \propto \frac{F\lambda}{A_{ul}}$$

where N_u is the column density of H_2 in the upper level of excitation energy E_u , of an observed line which has wavelength λ , flux F , and transition probability A_{ul} (quantities are listed in Table 2); g is the degeneracy given by the product of the rotational and spin degeneracies $g_J \times g_S$ where $g_J = 2J + 1$ and $g_S = 3$ for odd J and 1 for even J . In the optically thin regime, these equations can be used to estimate the mass of hot gas M_{H_2} from the line luminosity L since

$$L = f_u A_{ul} \frac{hc}{\lambda} \frac{M_{H_2}}{m_{H_2}}$$

where f_u is the fraction of hot H_2 in the upper level of the line, and m_{H_2} is the mass of a hydrogen molecule. Using the normalisation from Scoville et al. (1982) for gas thermalised at 2000 K that for the $v = 1, J = 3$ level $f_u = 0.0122$, the hot gas mass can be estimated from the 1-0 S(1) line luminosity as

$$L_{1-0S(1)}(L_\odot) = 620 M_{H_2}(M_\odot)$$

In the population diagram, parameters were derived by minimising chi-square; confidence regions were determined by systematically varying each of T and f_{UV} (which are not necessarily independent) while simultaneously optimising the absolute scaling, until chi-square had increased by one standard deviation. For the NE nucleus $T = 1500 \pm 60$ K and $f_{UV} = 0.19 \pm 0.02$; for the SW nucleus $T = 2460 \pm 410$ K and $f_{UV} = 0.29 \pm 0.12$.

For a second model we attempted to fit two thermal components, since it is not implicitly ruled out by the data. For the NE nucleus, the reduced chi-square $\chi_\nu^2 = 1.96$, rather larger than the expectation value of $\langle 0.91 \rangle$ for 7 degrees of freedom. As well as this statistical argument, there is a physical reason against the model: the temperatures derived are 1200 K and 5260 K. While the former only varies by ± 100 K, the 1σ limits on the latter encompass the range 4000–7600 K. Since H_2 rapidly dissociates at temperatures above 4000 K, it is not possible to get a strong thermal spectrum at the temperatures indicated here. Thus we can rule out this model for the NE nucleus. For the SW nucleus, the two-component thermal model effectively reduces to a single thermal component which is itself simply a subset of the previous thermal plus non-thermal model. The value $\chi_\nu^2 = 1.95$ for a single thermal component supports the result of the thermal plus non-thermal model above that a pure thermal model is unlikely.

4.2.1. *UV Fluorescence*

If the non-thermal H_2 component arises in photo-dominated regions due to UV fluorescence at the edge of HII regions, the models of Puxley et al (1990) can be used to constrain the compactness of the star forming regions. The diagnostic needed is the fluorescent 1-0 S(1)/Br γ ratio, which we estimate to be 0.35 ± 0.04 (NE) and 0.16 ± 0.07 (SW); the latter ratio may be intrinsically higher if any of the Br γ is related to the AGN.

The ratios derived are rather higher than expected, and the models suggest that they are typical of star formation which is either fairly diffuse or relatively evolved (so the most massive ionising stars are no longer present), both of which seem rather unlikely. The former option contradicts observations that intense star formation appears to occur mostly in compact clusters 2–3 pc across with masses up to $10^6 M_\odot$ (eg Meurer et al. 1995) which would have ionising fluxes on the order of 10^{52} – 10^{53} sec^{-1} and hence, according to the model, rather small ratios. Indeed, Davies et al. (1998) found that the 1-0 S(1)/Br γ ratios of such clusters, averaged over the central few tens of parsecs in the nuclei of blue compact dwarf galaxies, were $\lesssim 0.1$. The latter option can be refuted by considering the Br γ equivalent width, $W_{\text{Br}\gamma}$, which implies a maximum age of 50 Myr for the clusters dominating the $2 \mu\text{m}$ continuum. Since this time span is only greater than the main sequence lifetime of stars more massive than $\sim 15 M_\odot$, many highly ionising stars will still be present, implying a low UV fluorescent 1-0 S(1)/Br γ ratio. The high HeI/Br γ ratios of 0.62 ± 0.04 and 0.47 ± 0.03 in the NE and SW nuclei respectively, also point towards very hot stars. Although not a unique indicator of stellar temperature (due to resonant and, at high densities, collisional effects, Shields 1993), such high values suggest $T_{\text{eff}} = 30$ – $40 \times 10^3 \text{ K}$ equivalent to stars of mass 15–30 M_\odot . As discussed below, some other process as well as UV fluorescence is probably needed to account for much of the non-thermal H_2 emission.

At high densities, $\gtrsim 10^5 \text{ cm}^{-3}$, collisional effects will tend to thermalise the H_2 molecules, altering the emission spectrum. This means that in principle UV fluorescence can also give rise to a spectrum that is apparently thermal, an effect used to explain the anti-correlation between the ratio of 2-1 S(1)/1-0 S(1) and the intensity of 1-0 S(1) (Usuda et al. 1996). Here, since it appears already that fluorescence can account for only part of the weak non-thermal 1-0 S(1) emission, it is unlikely to contribute more than a few percent to the much stronger thermal part.

4.2.2. *X-ray Excitation*

In order to determine whether X-ray irradiation can be a potential source of H_2 line excitation we need to estimate the 1–100 keV X-ray flux. The 0.1–2.0 keV X-ray luminosity has been determined by Wang et al. (1997) who analysed the X-ray emission from Mkn 266, making use of both the High Resolution Imager (HRI) and Position Sensitive Proportional Counter (PSPC) instruments on *ROSAT* to identify a soft diffuse halo as well as 3 harder compact sources. They found that one associated with the SW nucleus has a luminosity of 1.3 – $7.5 \times 10^{41} \text{ ergs s}^{-1}$ and

the NE nucleus has $0.9\text{--}5.1 \times 10^{41}$ ergs s $^{-1}$, depending on the absorbing hydrogen column density ($N_{\text{H}} = 0.016 \text{ \& } 0.3 \times 10^{22}$ cm $^{-2}$). However, they found that only thermal plasma models fit the data satisfactorily, an unusual result given that the SW nucleus hosts an AGN for which the canonical hard X-ray spectrum is a power-law $F_{\nu} \propto \nu^{\alpha}$ with index $\alpha = -0.7$. That there is no way to be sure which sources seen with the HRI correspond to which parts of the spectrum observed with the PSPC adds confusion. Since the SW nucleus contributes $\lesssim 20\%$ of the total counts, these may not have much impact on the 0.1–2 keV spectrum, and it is possible that the spectrum at energies lower than 2 keV is dominated by star-formation, while a Seyfert-like power-law would only emerge at higher energies. This is seen in some Seyfert 2s, such as Mkn 3 (Serlemitsos, Ptak & Yaqoob 1996).

This could well be the case for the SW nucleus, where we make the reasonable assumption that the AGN dominates the X-ray luminosity, so we can put very comfortable upper limits on the extrapolated 1–100 keV luminosity. By normalising the 0.1–2 keV region of a power-law model with the same N_{H} to the entire HRI count rate of the source, we can derive this upper limit as $L \sim 12 \times 10^{41}$ ergs s $^{-1}$. The specific case of X-ray illumination of dense tori around AGN was modelled by Krolik & Lepp (1989), who found that $L_{1-0\text{S}(1)} \sim 10^{-4} L_{\text{X-ray}}$ for Seyfert 1s and $L_{1-0\text{S}(1)} \sim 10^{-5} L_{\text{X-ray}}$ for Seyfert 2s. The 1-0 S(1) luminosity in a 5'' aperture (similar to that used to estimate the X-ray flux from this source) around the SW nucleus in our line image is around 2 orders of magnitude larger than predicted for X-ray excitation alone. An additional argument against significant X-ray excitation is the offset of ~ 500 pc between the peak H $_2$ and AGN positions.

If the NE nucleus also hosted an AGN, similar arguments would apply. If, on the other hand, we assume the X-rays are associated with star-formation (eg supernovae or binaries), we should use the luminosities directly from Wang et al. (1997). The simplest models of H $_2$ for this case are those of Lepp & McCray 1983. They predict that the total 1-0 S(1) luminosity is 0.25% of the X-ray luminosity, ie we would expect $0.6\text{--}3 \times 10^5 L_{\odot}$ of 1-0 S(1) emission, whereas the total luminosity observed in 5'' is $12.5 \times 10^5 L_{\odot}$. Thus X-ray excitation is expected to contribute 5–25% of the 1-0 S(1).

4.2.3. Shock Excitation

Shocks can be very effective at exciting H $_2$ molecules and here we consider models of fast & slow J & C shocks from Burton et al (1990). These were originally tailored to the supernova remnant IC 433, but the general results have a much wider application.

fast J shock ($100\text{--}300$ km s $^{-1}$) would dissociate the molecules, which then reform downstream on grain surfaces via formation pumping (Mouri & Taniguchi 1995). The observed spectrum would be similar to that of UV fluorescence as the molecules are created in energetic states which then decay radiatively (see Table 1 in that paper). These authors give the emissivity

(photons emitted per molecule formed) of 1-0 S(1) as ~ 0.02 , requiring the shock(s) to pass through $1500 M_{\odot} \text{ yr}^{-1}$ near each nucleus if 50–70% of the fluorescent emission is due to fast J shocks. Additional tests are needed before we can confirm or rule out this process. That an equal flux of Br γ would be produced does not contradict the observations, as long as some other process can make up the bulk of the Br γ without producing significant H $_2$ emission. Observations of the J and H band [Fe II] lines would be useful, as fast J shocks would destroy grains, enhancing the gas-phase Fe $^+$ abundance so that the line strength becomes comparable to 1-0 S(1) (Hollenbach & McKee 1989).

slow J shock could be possible and would not dissociate the molecules. Shock velocities in the range $v_s = 5\text{--}15 \text{ km s}^{-1}$ result in strong H $_2$ lines and a post-shock temperature $T = (3900 \text{ K})(v_s/10 \text{ km s}^{-1})$ (Shull & Draine 1987). However, in normal ionisation fractions, magnetic field strengths, and gas densities such shocks are expected to revert to C type (Hollenbach, Chernoff & McKee 1989).

fast C shock with $v_s \sim 40 \text{ km s}^{-1}$ heats the gas to $\geq 2000 \text{ K}$ (dependent on v_s) and produces strong H $_2$ line emission, which could easily account for the bulk of the thermal excitation. We estimate a mass of 1600 and 1000 M_{\odot} of hot gas are needed near the NE and SW nuclei. The flow time through the hot shock structure of $\sim 100 \text{ yr}$ (Draine et al. 1983), then suggests that 10 and 16 $M_{\odot} \text{ yr}^{-1}$ of gas must be shocked to sustain the line’s thermal luminosity.

slow C shock is unlikely as the peak temperature is rather low, $\leq 300 \text{ K}$, resulting in very weak H $_2$ emission. This would contradict the strong observed emission and derived temperatures.

We have considered the various mechanisms which might give rise to the H $_2$ emission in the vicinity of each nucleus ($R \lesssim 1 \text{ kpc}$), and find the simplest solution is that outlined below. The non-thermal emission is a combination of UV fluorescence (1-0 S(1)/Br $\gamma \sim 0.1$) and fast 100–300 km s^{-1} dissociative J shocks (1-0 S(1)/Br $\gamma \sim 1$), the latter probably accounting for 50–70% with the ratios adopted here and heating $\sim 1500 M_{\odot} \text{ yr}^{-1}$ gas near each nucleus. The thermal emission is due in part to X-ray heating but mostly fast 30–50 km s^{-1} non-dissociative C shocks, heating only $\sim 10\text{--}16 M_{\odot} \text{ yr}^{-1}$ of dense clouds. In terms of the 1-0 S(1) line, the contributions are approximately: for the NE nucleus 5–25% X-ray heating, $< 5\%$ UV fluorescence, 15–20% fast J shocks, 55–75% fast C shocks; for the SW nucleus $< 20\%$ UV fluorescence, 10–30% fast J shocks, 70% fast C shocks.

4.3. Spatial Analysis

In order to reach sufficient signal-to-noise for the above analysis, we examined only the integrated flux around the nuclei and ignored the morphology. A spatial analysis of the brighter features along the slit can also be fruitful, as is apparent from Fig 6. The upper row shows the continuum, 1-0 S(1) line and Br γ line fluxes along the slit from the SW nucleus (left) to the NE

nucleus (right). That the (relative) line fluxes do not exactly tally with those given in Table 1 is due to different apertures: the data in the table were extracted from a $5''$ circular aperture, those in the figure from $0.61'' \times 1.22''$ boxes. Also, no structures less than $1\text{--}1.5''$ will be visible, so the details seen in the images in Fig 1 are not apparent.

The lower row of the figure is more interesting: it shows that the ratios of 1-0S(1) to both $\text{Br}\gamma$ and the continuum *increase* away from the nuclei. Thus although the H_2 emission right in the nuclei may be associated with $\text{Br}\gamma$ and the $2\mu\text{m}$ continuum (eg via star formation processes), that more than $\sim 1''$ away is not. Remarkably the ratios remain high even $2\text{--}3''$ away, a physical distance of $1\text{--}1.5$ kpc, although the surface brightness is very low.

4.4. Extinction

The extinctions derived from the $\text{H}\alpha/\text{H}\beta$ ratio in Veilleux et al. (1995), and also using the $\text{H}\alpha/\text{Br}\gamma$ ratio, are very small ($A_V \lesssim 3$, Table 1). In the case of the NE nucleus, they are almost the same and suggest a correct measure for the total extinction. However, for the SW nucleus, the A_V found using the $\text{Br}\gamma$ line is significantly larger, an indication that we are probing to greater optical depths with the less-absorbed near-infrared line. Additionally continuum fits to the spectra give $A_V \sim 4$, remarkably consistent (especially in the K-band where $A_K = 0.1A_V$) given the way they were determined, and that they probe the stellar continuum rather than the excited gas. Lastly, we measured the $\text{Pa}\alpha/\text{Br}\gamma$ ratio, which yielded somewhat higher values of $A_V \sim 7$ for the NE and $A_V \sim 13$ for the SW nuclei; we must disregard these since the $\text{Pa}\alpha$ lines are seen at very low ($<40\%$) atmospheric transmission, and systematic errors of only $10\text{--}30\%$ would bring them in line with the other estimates.

5. Discussion

In this section we draw together the various lines of evidence that we have examined, in an attempt to paint a consistent picture of the events occurring in Mkn 266.

5.1. North East Nucleus

The NE nucleus is classified from its optical spectrum as a LINER by Osterbrock & Dahari (1983) and as a Seyfert 2 by Veilleux et al. (1995). Some confusion is unavoidable as explanations for LINER spectra are typically either weak AGN or shock excitation, maybe due to a starburst (Filippenko 1996). Both we (at $2\mu\text{m}$) and MGAH (at $2\text{--}20$ cm) have found that this nucleus is resolved on scales of several hundred parsecs, making an AGN an unlikely proposition. Additionally, Smith et al. (1998) found evidence for simple structure at VLBI 18 cm scales. The

flux they detected was 4.5 mJy, only 20% of that in the entire nucleus, suggesting that even if there is an AGN component, it certainly cannot dominate the power output. Instead we assume that all the Br γ is due to recent star formation, and using models of Leitherer et al. (1995) we estimate the supernova rate (ν_{SN}), K-band luminosity (L_{K}), and bolometric luminosity (L_{bol}) with which it is likely to be associated. We employ models with solar metallicity and a Salpeter (slope 2.35) initial mass function (IMF) in the range 1–100 M_{\odot} .

If active star formation occurred over a short period and has since evolved passively, then it must be very young as Br γ flux and equivalent width fall off very quickly with time; the directly measured Br γ equivalent width ($W_{\text{Br}\gamma}$) of 10 Å (in a 2'' aperture) provides an upper limit to the age. This is an unrealistic number to use since at least some of the continuum is from an old underlying population (as evidenced by the extended continuum): decomposition of the deconvolved image suggests that in the central 2'', roughly 70% of the continuum is from the core and the rest extended. Additionally in Section 4.1 we showed that supergiants make up \sim 25% of the continuum. Taking these two cases as the extremes implies that the $W_{\text{Br}\gamma}$ associated with the most recent episode of star formation should lie in the range 15–40 Å. This constraint gives a range of 4.5–6.5 Myr, consistent with the CO index $CO_{\text{ph}} = 0.12$. Such a young age implies $3\text{--}8 \times 10^7 M_{\odot}$ of stars would have had to form effectively instantaneously ($\lesssim 1$ Myr) in order to reproduce the observed Br γ flux. We would then predict the parameters $\nu_{\text{SN}} = 0.03\text{--}0.08 \text{ yr}^{-1}$, $L_{\text{K}} = 2\text{--}7 \times 10^8 L_{\odot}$, and $L_{\text{bol}} = 3\text{--}6 \times 10^{10} L_{\odot}$.

Models for continuous star formation may also be appropriate for this object, and a plausible scenario might invoke ‘punctuated star formation’ in which clusters of $10^5\text{--}10^6 M_{\odot}$ formed at different times over this period. $W_{\text{Br}\gamma} = 15\text{--}40 \text{ \AA}$ then implies an age of 60–500 Myr (or more), during which entire period the stars have formed with an average rate of $1.7 M_{\odot} \text{ yr}^{-1}$ (ie, a few clusters every Myr). 60 Myr is the time at which the maximum supernova rate $\nu_{\text{SN}} = 0.03 \text{ yr}^{-1}$ is reached and thereafter sustained. Unfortunately the CO index does not constrain the age range, although both L_{K} and L_{bol} should since they increase slowly with time as more late-type giants are accumulated. Yet even after 500 Myr the model predicts only $L_{\text{K}} = 5 \times 10^8 L_{\odot}$ and $L_{\text{bol}} = 4 \times 10^{10} L_{\odot}$.

The parameters for these two models are summarised in Table 3 as Models 1 and 2 respectively, and are compared with observed quantities. For these we used the K-band luminosity from this paper and, as above, suppose that somewhere in the range 25–70% of that in 2'' comes from the starburst. The bolometric luminosity is the infrared (8–1000 μm) luminosity taken from Sanders et al. (1991). We assume that each nucleus contributes in rough proportion to its Br γ and X-ray fluxes, amounting to 30–50% for the NE nucleus. The model predictions for these two quantities are factors of 3–4 less than those observed.

The supernova rate ν_{SN} has an even larger discrepancy. To estimate it from the 20 cm continuum we used the relation derived by Condon & Yin (1990), between non-thermal radio continuum and supernova rate. By considering independent estimates of these for the Galaxy they

found:

$$L_{\text{NT}}[\text{W Hz}^{-1}] \sim 1.3 \times 10^{23} (\nu[\text{GHz}])^{-0.8} \nu_{\text{SN}}[\text{yr}^{-1}]$$

This is very similar to the relation derived for M82 by Huang et al. (1994), who find a coefficient of $1.1 \pm 0.5 \times 10^{23}$ for that galaxy by considering the cumulative number of sources as a function of increasing diameter. Additionally, by using the temporal behaviour of the bright SN1979c in M100 as a template, Colina & Pérez-Olea (1992) derived a coefficient of 0.9×10^{23} for the same equation. So this relation appears to be quite robust, whether applied to the Galaxy or to the rather different environment of starbursts. From the 20 cm radio continuum (MGAH) which has a spectral index of 0.6 and hence will be dominated by the non-thermal component at this wavelength, we derive $\nu_{\text{SN}} = 0.45 \text{ yr}^{-1}$.

These calculations provide a strong indication that the starburst scaling obtained from the Br γ flux is too small by an order of magnitude. There are potentially several ways around this problem. A number of authors have suggested that the IMF might be truncated or have a steep slope, both of which reduce the number of most massive stars. These two cases were also modelled by Leitherer et al. (1995), and $W_{\text{Br}\gamma} = 20 \text{ \AA}$ gives maximum ages of 30 Myr (Miller-Scalo IMF with slope 3.3) and 11 Myr (upper mass limit set to $30 M_{\odot}$). Although the normalisation of the model to the observed ionising flux then increases, the predicted supernova rate actually decreases. For the truncated IMF it is because the age is so small that many of the progenitor stars are too young to produce supernovae; for the steep IMF it is mainly because there are fewer supernova progenitors.

The required effect of reducing the observed Br γ flux could also be achieved if there was dust internal to the ionised nebulae, which then competes for Lyman continuum (Lyc) photons. Perhaps more likely is that if the molecular clouds have been shredded by multiple supernovae, the nebulae may be density bounded so that many of the Lyc photons escape. With the measured $A_V \sim 2$ more than 90% of these photons would be mopped up by dust in the ISM, contributing to the far-infrared flux without increasing the observed UV. In either case the hydrogen recombination line strengths would be reduced by the same factor. An intriguing side-effect is to alter the ratio of H α or H β to the high ionisation species such as [OIII]. Since lines with higher ionisation potentials are produced deeper in the nebula, their strengths will not be affected if the nebula is density bounded (except in rather extreme cases). Such an effect could account for the high ratio of [OIII]/H β measured by Veilleux et al. (1995) leading to their classification as a Seyfert. We can hypothesise a ‘intrinsic’ Br γ flux (ie the one we ought to measure if all the Lyc photons ionised H I), which would be many times larger than that observed. However, this does not solve our problem since $W_{\text{Br}\gamma}$ must also increase by the same factor, forcing us again to adopt a very young starburst age.

One remaining hypothesis involving star formation is that at some point 10–30 Myr ago a catastrophic event may have triggered a single highly intense burst of activity, forming $\sim 7 \times 10^8 M_{\odot}$ during this period. The starburst would now have evolved enough that it contributes little to the current Br γ luminosity (1–2%) while accounting for the radio continuum, L_K , and

L_{bol} . This is shown as Model 3 in Table 3. The corollary is that this leaves almost no age constraints on the star formation responsible for the $\text{Br}\gamma$. However, the difficulty here is that the radio and $2\ \mu\text{m}$ continua trace out different regions so it seems unlikely they could originate from the same episode of star formation.

A different approach is to consider an alternative origin for the synchrotron radiation – which must nevertheless arise from electrons accelerated by shocks since we have shown that an AGN is not a proposition. Perhaps the two most important pieces of evidence are: (1) the 1-0S(1) and radio continuum appear to be related to each other because of their shock origin, and (2) although the radio continuum is resolved, both it and the 1-0S(1) are very compact (on scales of $0.4''$) – and, crucially, *more so* than the $2\ \mu\text{m}$ continuum ($0.7''$). Our spectra show that the $2\ \mu\text{m}$ continuum is dominated by late-type stars, and presumably traces out the region of recent star formation. We argue that perhaps the radio and 1-0S(1) are *not* directly associated with the star formation. Although the spatial scales are too small to make a definitive statement, the morphology does appear to be similar to that of NGC 6240 where the gas has settled between the two continuum nuclei and is radiating strong thermal 1-0S(1) emission (van der Werf et al. 1993, Sugai et al. 1997b, Tacconi et al. 1999). If NGC 6240 were moved away so that its nuclei, instead of being $1.5''$ apart, were separated by only $0.5''$, it would begin to look like Mkn 266 NE. We speculate whether Mkn 266 NE could itself consist of two or more (unresolved) continuum nuclei with gas settling between them. As the models we have considered imply, star formation has occurred recently in these nuclei, but the supernova rate is very low so essentially all the radio continuum originates in the settling gas. A serious difficulty with such an interpretation is that Mkn 266 NE has a 3.6 cm intensity (scaled from the 2 cm, MGAH) of 7.0 mJy within $0.3'' \times 0.4''$, while NGC 6240 has diffuse 3.6 cm emission at the level of 0.2 mJy in a $0.23'' \times 0.32''$ beam (Colbert et al. 1994) – some 35 times fainter. Since we cannot invoke an AGN, it is hard to conceive of a method to produce so much more non-thermal radio emission without reverting to fast shocks. Bell (1978) showed that the radio emissivity of shocked gas is strongly dependent on the shock velocity v_s :

$$\epsilon(\nu) \propto \left(\frac{n_e}{\text{cm}^{-3}}\right) \left(\frac{B}{10^{-4}\text{ G}}\right)^{\alpha+1} \left(\frac{v_s}{10^4\text{ km s}^{-1}}\right)^{4\alpha} \left(1 + \left[\frac{v_s}{7000\text{ km s}^{-1}}\right]^{-2}\right)^{\alpha} \left(\frac{\nu}{\text{GHz}}\right)^{-\alpha}$$

So for a typical spectral index of $\alpha = 0.8$ we find that $\epsilon(\nu) \propto v_s^{1.6}$ for $v_s \lesssim 2000\text{ km s}^{-1}$; while $\epsilon(\nu) \propto v_s^{3.2}$ for $v_s \gtrsim 7000\text{ km s}^{-1}$. To produce such intense synchrotron emission requires shocks with speeds of several thousand km s^{-1} , 3–10 times faster than the 300 km s^{-1} seen in the CO line in NGC 6240 by Tacconi et al. (1999). However, in NGC 6240 higher velocities than in the CO line were observed in 1-0S(1) which has a FWHM of 550 km s^{-1} and FWZI of 1600 km s^{-1} (van der Werf et al. 1993). Also, in Section 4.2 we saw that the fraction of H_2 excited by dissociation due to fast shocks is much higher in Mkn 266 than in NGC 6240; and to account for this ~ 100 times more gas in Mkn 266 is shocked at high velocities than at the low velocities expected in dense molecular clouds. Bell’s equation shows that, keeping all other parameters the same, increasing the shock velocity from 300 km s^{-1} to 3000 km s^{-1} would increase the synchrotron intensity by a factor of

30, similar to the observed difference between NGC 6240 and Mkn 266. It does not seem totally unreasonable then to extrapolate from NGC 6240 to a more extreme environment in Mkn 266 NE: if gas has settled into a disk structure on scales several times smaller than in NGC 6240, the velocities required to support it centrifugally will be many times greater and this could give rise to the fast shocks required to produce the intense synchrotron emission. High resolution observations of the CO in this nucleus will be needed to decide whether this speculation is indeed borne out.

One final point to consider is the existence of faint but very extended wings out to at least 1–1.5 kpc in the 1-0S(1), as indicated in Fig 2. The lower limits to the S(1)/Br γ ratio and the high S(1) equivalent width indicated in Fig 6 imply an origin not associated with star formation. A plausible alternative is that the lines are excited by shocks which are driven into clouds in the turbulent medium of the X-ray halo.

5.2. South West Nucleus

This nucleus has also been identified as a LINER (Veilleux et al. 1995) and Seyfert 2 (Osterbrock & Dahari 1983). The classification as a LINER rested solely on the ratio [OIII]/H β = 1.4 because the diagrams used to distinguish LINERs, Seyferts, and starbursts all plotted this value, against the ratios of [NII], [SII], and [OI] to H α . Evidence for an AGN comes from MGAH who observed an unresolved radio core in the SW component using a beamwidth of 0.3'' \times 0.4'', and our deconvolved continuum image. An additional line of reasoning put forward by Wang et al. (1997) is that photoionisation by the hard radiation field of an AGN is needed to explain both the luminosity of the large-scale optical emission line nebula as well as the line ratios. As discussed in Section 3, based on the 2 μ m continuum we would argue for a combination of Seyfert plus starburst.

The surrounding emission, extending linearly about 1'' both north and south (radio as well as infrared) would be due to star formation. The Br γ follows the distribution to some extent, although the resolution is rather poor; for example, the extension to the east is apparent in both continuum and line images and may be due to an extranuclear HII region. Unfortunately, a quantitative analysis is not possible with the current spatial resolution, since we cannot properly separate the AGN and starburst contributions.

More interesting is the H $_2$, which peaks to the north east between the galaxies in a region without any associated Br γ or continuum, and 500 pc from the nucleus. This would seem to rule out any connection with either the AGN or star formation. In Section 4.2 we showed that 70% of the 1-0S(1) emission in this nucleus was thermally excited and deduced that it arose mostly in \sim 40 km s $^{-1}$ C shocks. Together these suggest that it may be due to shocks resulting from the interaction being driven into clouds. Both we and Veilleux et al. (1995) found a radial velocity difference between the nuclei of 50 km s $^{-1}$, setting a lower limit on the speed of the interaction. It is likely that the actual speed is faster, but shock speeds similar to that required can be produced

when a high speed shock in a low density medium encounters a high density medium, the process favoured for the H_2 excitation in NGC 6240 by van der Werf et al. (1993) and Sugai et al. (1997b). However, it is not possible to comment here on whether it is due to the global interaction, or if it results from the gas dynamics more closely associated with the SW nucleus.

5.3. The Central Radio Continuum

One of the puzzling observations of Mkn 266 is the non-thermal radio continuum midway between the nuclei, stronger than the extended emission in the SW nucleus and accounting for more than 1/4 of the total 20 cm emission (MGAH). What makes this so surprising is that there is no evidence for any other enhanced emission *of any sort* at this position.

MGAH argued that it could result from shocks as clouds collide near the interface of the gas disks. Our most severe observational constraint on this model is the non-detection of 1-0S(1) in the locale, at a 5σ limit of $10^{-18} \text{ W m}^{-2}$ (in a $5''$ aperture, similar in size to the $3'' \times 7''$ radio emission). The MGAH scenario is ideally suited to the interacting galaxy model of Jog and Solomon (1992), which describes pairs of gas rich spiral galaxies colliding at 300 km s^{-1} . This model has an important addition to previous models (eg Harwit et al. 1987) which have invoked collisions between GMCs to explain the observations. The authors note that GMCs have a low volume filling factor $f_{\text{GMC}} = 0.01$ and so are unlikely to collide; it is the HI clouds with $f_{\text{HI}} = 0.1$ which collide. The GMCs are assumed to have a core radius of 25 pc with an average density $n_{\text{H}_2} = 100 \text{ cm}^{-3}$; the HI clouds are given a radius of 5 pc and an average density $n_{\text{H}} = 20 \text{ cm}^{-3}$, but with the larger filling factor, the total mass is the same as the H_2 .

The fast shocks in the HI clouds are slowed in the denser GMCs to $\sim 50 \text{ km s}^{-1}$, which are still nevertheless highly supersonic; the compression timescale of $\sim 2 \times 10^4 \text{ yr}$ then implies that in total only about 10% of the GMC gas is shocked. The cooling timescale is on the order of 100 yrs (Drain, Roberge & Dalgarno 1983), so only 0.5% of the shocked H_2 is radiating at any time.

At a distance of 115 Mpc, and taking the line-of-sight dimension as an average of the others, the volume over which the radio continuum is emitted is 24 kpc^3 . The H_2 mass inside this would then be $10^9 M_{\odot}$, of which $5 \times 10^5 M_{\odot}$ would be hot – roughly the same amount as in NGC 6240 (Sugai et al. 1997b), and about 500 times more than is implied by our 5σ upper limit to the 1-0S(1) line. Even allowing for large uncertainties in the parameters and timescales, invoking shock excitation in clouds induced by the interaction appears unlikely.

We offer a slightly different interpretation. Wang et al. (1997) have argued that X-ray and optical emission line observations point towards a radial outflow of gas at several hundred km s^{-1} which has swept up much of the ISM, and they conclude that the NE starburst and SW AGN play comparable roles in photoionising the nebula. At distances of a few kpc, the outflow velocity is $\sim 300 \text{ km s}^{-1}$. Our hypothesis is that the radio continuum traces the interface between the expanding shock fronts from the two nuclei. When added to the relative velocity of the galaxies,

the relative velocities of these shocks will be approaching 1000 km s^{-1} . Copious quantities of non-thermal radio emission will be produced even if the density of the shocked material is fairly low, but there will be no 1-0S(1) and little hydrogen recombination flux as the gas is heated to 10^6 – 10^7 K. A test of this would be to observe the region with high spatial resolution in the 0.1–2 keV range, to see if there is a local increase in the temperature of the X-ray emitting gas over the ambient temperature in the bubble of 10^6 K.

6. H₂ Excitation: The Wider Perspective

The classical case of H₂ emission occurring between the nuclei in a merger is that of NGC 6240 (Herbst et al. 1990, van der Werf et al 1993). The H₂ level population is consistent with solely thermal excitation and, combined with the absence of [FeII] in the same region, indicates that the *observed* emission arises from non-dissociative shocks, occurring as a result of the merging process (Sugai et al. 1997b). Recent CO radio observations (Tacconi et al. 1999) have confirmed the presence of $2\text{--}4 \times 10^9 M_{\odot}$ of molecular gas concentrated here.

Other radio CO observations of a number of galaxies at 1–3'' resolution by Gao et al. (1997) tend to support this more generally, and Scoville et al. (1997) argue that 2/3 of the molecular gas in Arp 220 relaxing into such a disk is consistent with scenarios in which gas in merging systems settles into the centre faster than the stellar nuclei. They argue that efficient removal of angular momentum from the observed dense centrifugally supported disk could play an important role in the evolution of powerful starbursts/AGN. They estimated a mass of $5.4 \times 10^9 M_{\odot}$ in the disk with a mean density of $2 \times 10^4 \text{ cm}^{-3}$. Based on the model of Jog & Solomon (1992) discussed in Section 5.3, we estimated a ratio of cold to hot (shocked) molecules of 2000. This is not so different from the ratio of found in NGC 6240: Tacconi et al. (1999) estimated the cold H₂ mass to be $2\text{--}4 \times 10^9 M_{\odot}$, while Sugai et al. (1997b) found a cold H₂ mass of $2 \times 10^5 M_{\odot}$, yielding a ratio of 10^4 . Even for this case the 1-0S(1) emission should be easily observable. For example, for a merger at 200 Mpc to produce a 1-0S(1) flux of $10^{-18} \text{ W m}^{-2}$, an H₂ disk mass of only $\sim 2 \times 10^7 M_{\odot}$ is needed. Given the examples of Arp 220 and NGC 6240, this seems a perfectly feasible proposition for any of the luminous infrared galaxies (almost all at distances < 200 Mpc) observed by Sanders et al. (1991), in which the CO luminosity implies total H₂ masses in the range 10^9 – $10^{10} M_{\odot}$.

We have now observed several other such systems similar to NGC 6240 by targeting close mergers, although with current observations it is not possible to say whether the gas has formed a disk structure in these galaxies. These include Mkn 551 (Sugai et al 1997a), Mkn 266 (here), and Mkn 496 (Sugai et al. 1999a). Also, the line images of NGC 3256 (Kotilainen et al 1996) suggest that there is an enhancement of 1-0S(1) between the two nuclei with respect to both the Br γ and [FeII], which fall to a minimum. This phenomenon is not limited to the luminous infrared galaxies, and has also been observed in some blue compact dwarf galaxies (II Zw 40, NGC 5253, and He 2-10, Davies et al. (1998)) where again the 1-0S(1) bears little or no resemblance to the Br γ or $2\mu\text{m}$ continuum. However, the 1-0S(1) surface brightness is low in these interacting systems, and

it could only be detected because they are all nearby (<10 Mpc). The more luminous galaxies with correspondingly larger gas masses do form a better sample for further study, and although such emission is not always observed (eg Arp 299, Sugai et al 1999b), it may nevertheless be a relatively common phenomenon and should be observable with the current generation of infrared instrumentation.

7. Summary & Conclusions

We have presented near infrared data on Mkn 266 consisting of $2\mu\text{m}$ continuum, and $\text{Br}\gamma$ and 1-0S(1) emission line images, as well as K-band spectra. These are analysed in conjunction with data from the literature, primarily the radio continuum (MGAH).

There are 3 main observations to note from the images.

- (1) In the NE (LINER) nucleus the 1-0 S(1) is similar in size ($\lesssim 0.45''$) to the radio continuum, but more compact than the $2\mu\text{m}$ continuum ($0.7''$).
- (2) In the SE (AGN+starburst) nucleus, the 1-0 S(1) is offset from the continuum emission by $0.9''$ (500 pc), and has no associated $\text{Br}\gamma$ emission or radio continuum.
- (3) Midway between the two components where there is a region of strong radio continuum, we find no enhanced near infrared line or continuum emission at all.

From our analysis of the spectra we note the following.

- (1) By fitting stellar templates to parts of the spectra away from emission lines, we are able to remove all the absorption features, and hence measure the fluxes of even weak emission lines. Simultaneously we find that 20–25% (NE) and 50% (SW) of the continuum is due to supergiants, the rest originating in late type giant stars.
- (2) Level population diagrams of the hot H_2 molecules indicate that in the NE and SW nuclei respectively, $81\pm 2\%$ and $71\pm 12\%$ of the 1-0 S(1) is thermally excited (to temperatures of 1500 ± 60 and 2460 ± 410 K), mostly by ~ 40 km s $^{-1}$ C-shocks. Additionally, much of the non-thermal emission may arise in faster dissociative J-shocks. Pure thermal models (with either one or two components of different temperatures) are effectively ruled out.
- (3) Although the 1-0 S(1) surface brightness is very low away from the nuclei, its ratio to $\text{Br}\gamma$ and the continuum remains high even out to $2\text{--}3''$.

The conclusions we draw are listed below.

NE nucleus: the extended nature argues against an AGN, but nor can any combination of star formation scenarios simultaneously account for the observations. Both the morphologies of the 1-0 S(1) and $2\mu\text{m}$ continuum, and the (predominantly) shock origin of the H_2 emission and radio continuum, are reminiscent of NGC 6240. We speculate that this nucleus may resemble NGC 6240 but on a smaller physical scale, and with the higher velocities that would necessarily occur in a smaller centrifugally supported disk.

SW nucleus: the morphologies suggest an AGN with circumnuclear star formation, but a quantitative analysis is not yet possible due to the small angular scales involved. Because the offset 1-0S(1) has no other associated emission it cannot originate in star formation, and may instead be due to shocks driven into clouds as a result of the interaction.

intermediate region: The lack of any enhanced 1-0S(1) emission suggests that the radio continuum cannot trace out regions shocked by the interaction. We propose that it indicates the interface between the expanding winds from each nucleus, where combined shock velocities would be high enough ($\sim 1000 \text{ km s}^{-1}$) that neither 1-0S(1) nor hydrogen recombination lines would be observed.

We thank the staff at UKIRT and the JAC for their help during the observing run. Some of the data were obtained as part of the UKIRT Service Programme, and we are grateful particularly to J. Davies who carried out the observations. The United Kingdom Infrared Telescope is operated by the Joint Astronomy Centre on behalf of the U.K. Particle Physics and Astronomy Research Council. RID acknowledges the support of the European Network on Laser Guide Stars which operates under the auspices of the Training and Mobility of Researchers programme. The authors thank Matt Lehnert for stimulating and helpful discussions.

REFERENCES

- Bell A., 1978. *MNRAS*, **182**, 443.
- Black J., van Dishoeck E., 1987. *ApJ*, **322**, 412.
- Burton M., Hollenbach D., Haas M., Erickson E., 1990. *ApJ*, **355**, 197.
- Colbert E., Wilson A., Bland-Hawthorn J., 1994. *ApJ*, **436**, 89.
- Colina L., Perez-Olea D., 1992. *MNRAS*, **259**, 709.
- Condon J., Yin Q., 1990. *ApJ*, **357**, 97.
- Davies R., Hackenberg W., Ott T., Eckart A., Rabien S., Anders S., Hippler S., Kasper M., Kalas P., Quirrenbach A., Glindemann A., 1999. *A&A*, **138**, 345.
- Davies R., Sugai H., Ward M., 1998. *MNRAS*, **295**, 43.
- De Marchi G., Clampin M., Greggio L., Leitherer C., Nota A., Tosi M., 1997. *ApJ*, **479**, L27.
- Doyon R., Joseph R., Wright G., 1994. *ApJ*, **421**, 101.
- Draine B., Roberge W., Dalgarno A., 1983. *ApJ*, **264**, 485.
- Filippenko A., 1996. In: *The Physics of LINERs in View of Recent Observations*, p. 17, eds Eracleous M., Koratkar A., Leitherer C., Ho L., ASP conf. ser. 103.
- Fioc M., Rocca-Volmerange B., 1997. *A&A*, **326**, 950.
- Förster-Schreiber N., 1999. *PhD thesis*, Ludwig-Maximilian-Universität, München.
- Gao Y., Greundl R., Hwang C., Lo K., 1997. In: *Galaxy Interactions at Low and High Redshift*, 519, eds Barnes J., Sanders D., IAU, Dordrecht: Kluwer.
- Goldader J., Joseph R., Doyon R., Sanders D., 1997. *ApJ*, **474**, 104.
- González Delgado R., Leitherer C., Heckman T., no M. C., 1997. *ApJ*, **483**, 705.
- Harwit M., Houck J., Soifer B., Palumbo G., 1987. *ApJ*, **315**, 28.
- Herbst T., Graham J., Beckwith S., Tsutsui K., Soifer B., Matthews K., 1990. *AJ*, **99**, 1773.
- Hollenbach D., McKee C., 1989. *ApJ*, **342**, 306.
- Hollenbach D., Chernoff D., McKee C., 1989. In: *Infrared Spectroscopy in Astronomy*, 245, ed. Kaldeich B., ESA SP-290).
- Huang Z., Thuan T., Chevalier R., Condon J., Yin Q., 1994. *ApJ*, **424**, 114.

- Jog C., Solomon P., 1992. *ApJ*, **387**, 152.
- Krolik J., Lepp S., 1989. *ApJ*, **347**, 179.
- Leitherer C., Heckman T., 1995. *ApJS*, **96**, 9.
- Lepp S., McCray R., 1983. *ApJ*, **269**, 560.
- Mazzarella J., Gaume R., Aller H., Hughes P., 1988. *ApJ*, **333**, 168.
- Meurer G., Heckman T., Leitherer C., Kinney A., Robert C., Garnett D., 1995. *AJ*, **110**, 2665.
- Mouri H., Taniguchi Y., 1995. *ApJ*, **449**, 134.
- Osterbrock D., Dahari O., 1983. *ApJ*, **273**, 478.
- Puxley P., Hawarden T., Mountain C., 1990. *ApJ*, **364**, 77.
- Sanders D., Scoville N., Soifer B., 1991. *ApJ*, **370**, 158.
- Scoville N., Hall D., Kleinmann S., Ridgway S., 1982. *ApJ*, **253**, 136.
- Scoville N., Yun M., Bryant P., 1997. *ApJ*, **484**, 702.
- Serlemitsos P., Ptak A., Yaqoob T., 1997. In: *The physics of LINERs in view of recent observations*, 70, eds Eracleus M., Korathar A., Leitherer C., Ho L., ASP, San Francisco.
- Shields J., 1993. *ApJ*, **419**, 181.
- Shull J., Draine B., 1987. In: *Interstellar Processes*, 283, eds Hollenbach D., Thronson H., Reidel.
- Smith H., Lonsdale C., Lonsdale C., 1998. *ApJ*, **492**, 137.
- Sternberg A., Neufeld D., 1999. *ApJ*, **516**, 371.
- Sugai H., Malkan M., Ward M., Davies R., McLean I., 1997a. In: *Galaxy Interactions at Low and High Redshift*, 92, eds Barnes J., Sanders D., IAU, Dordrecht: Kluwer.
- Sugai H., Malkan M., Ward M., Davies R., McLean I., 1997b. *ApJ*, **481**, 186.
- Sugai H., Davies R., Ishii M., Ward M. 1999a. MNRAS, submitted.
- Sugai H., Davies R., Malkan M., McLean I., Usuda T., Ward M., 1999b. *ApJ*, **in press**.
- Tacconi L., Genzel R., Tecza M., Gallimore J., Downes D., Scoville N., 1999. *ApJ*, **524**, 732.
- Usuda T., Sugai H., Kawabata H., Inoue M., Kataza H., Tanaka M., 1996. *ApJ*, **464**, 818.
- van der Werf P., Genzel R., Krabbe A., Blietz M., Lutz D., Drapatz S., Ward M., Forbes D., 1993. *ApJ*, **405**, 522.

Veilleux S., Kim D.-C., Sanders D., Mazarella J., Soifer B., 1995. *ApJS*, **98**, 171.

Wang J., Heckman T., Weaver K., Armus L., 1997. *ApJ*, **474**, 659.

Table 1. Mkn 266: Basic Quantities

Quantity	Unit	North-East Nucleus		South-West Nucleus	
		5''	2''	5''	2''
$2\ \mu\text{m}$ continuum ^a	[mJy]	9.43 ± 0.06	4.09 ± 0.03	14.07 ± 0.06	5.76 ± 0.03
	[mag]	12.10 ± 0.01	13.00 ± 0.01	11.67 ± 0.01	12.63 ± 0.01
Br γ line ^a	[$10^{-18}\ \text{W m}^{-2}$]	3.4 ± 0.4	2.6 ± 0.2	5.7 ± 0.4	2.8 ± 0.2
1-0 S(1) line ^a	[$10^{-18}\ \text{W m}^{-2}$]	3.2 ± 0.2	2.2 ± 0.1	2.3 ± 0.2	0.7 ± 0.1
1-0 S(1)/Br γ ^a		0.94 ± 0.13	0.85 ± 0.08	0.40 ± 0.05	0.25 ± 0.04
$W_{\text{Br}\gamma}$ ^a	[\AA]	5.7 ± 0.7	9.9 ± 0.8	6.3 ± 0.4	7.6 ± 0.5
A_V ^b	[mag]		2.3		0.9
A_V ^c	[mag]		2.7 ± 0.2		2.1 ± 0.2

^aMeasured in aperture given; errors are statistical, determined from noise in the images

^bfrom H α /H β ratio, Veilleux et al. (1995)

^cfrom H α /Br γ ratio, where H α is from Veilleux et al. (1995) and Br γ is measured in same region (3.7'' length section of a 2'' wide slit at position angle 36°). Errors are from Br γ flux only.

Table 2. relative line strengths & derived quantities^a

Line	Wavelength μm	E_u/k^b K	A_{ul}^b 10^{-7} s^{-1}	Relative strength	
				NE ^c	SW ^d
1-0 S(3) ^e	1.9576	8365	4.21	0.76	—
1-0 S(2)	2.0338	7584	3.98	0.33	0.46
2-1 S(3)	2.0735	13890	5.77	0.12	0.22
1-0 S(1)	2.1218	6956	3.47	1.00	1.00
2-1 S(2)	2.1542	13150	5.60	0.07	—
3-2 S(3)	2.2014	19086	5.63	0.04	—
1-0 S(0)	2.2235	6471	2.53	0.27	0.34
2-1 S(1)	2.2477	12550	4.98	0.12	0.24
1-0 Q(1)	2.4066	6149	4.29	0.81	0.65
1-0 Q(2)	2.4134	6471	3.03	0.28	0.35
1-0 Q(3)	2.4237	6956	2.78	0.69	0.85
Pa α ^f	1.8756			5.32	15.00
Br γ	2.1661			0.54	1.82
He I	2.0587			0.34	0.85

^aErrors are estimated from the residual continuum near each line. Due to poor atmospheric transmission and continuum subtraction shortwards of $1.9\mu\text{m}$, additional errors are present in this region and we are unable to measure the Br δ ($1.95\mu\text{m}$) or 1-0 S(4) ($1.89\mu\text{m}$) lines.

^bFor H_2 lines only; taken from the UKIRT Astro-Utilities page: <http://www.jach.hawaii.edu/JACpublic/UKIRT/astronomy/>

^cRatios are normalised to 1-0 S(1); 1σ errors are ~ 0.02

^dRatios are normalised to 1-0 S(1); 1σ errors are 0.05–0.07, except 0.11 for the Q-branch

^eAs there is no evidence for an AGN in the continuum, we have assumed there is negligible [Si VI] emission at $1.96\mu\text{m}$.

^fAs explained in *a*, there may be a large (10–30%) systematic error on this line making extinction estimates highly uncertain.

Table 3. Mkn 266 NE: Star formation models^a

Quantity	Unit	Model 1 ^b	Model 2 ^b	Model 3 ^c	Observed ^d	Note ^d
Age	10^6 yr	4.5–6.5	60–500	20		
Stellar mass	$10^7 M_{\odot}$	3–8	10–85	70		
ν_{SN}	yr^{-1}	0.03–0.08	0.03	0.40	0.45	from 20 cm radio
L_K	$10^8 L_{\odot}$	2.1–6.9	2.7–6.0	20.6	6–18	25–70% of flux in $2''$
L_{bol}	$10^{10} L_{\odot}$	3.3–5.7	2.9–3.8	12.0	9–15	30–50% of total L_{IR}

^aUsing the models of Leitherer et al. (1995)

^bInstantaneous (1) and continuous (2) models normalised to $\text{Br}\gamma$, assuming that 25% (lower ages) and 70% (higher ages) of the continuum within $2''$ is from the starburst.

^cInstantaneous model (3) scaled to ν_{SN} , L_K , and L_{bol} .

^dThe quantities measured, and where they came from

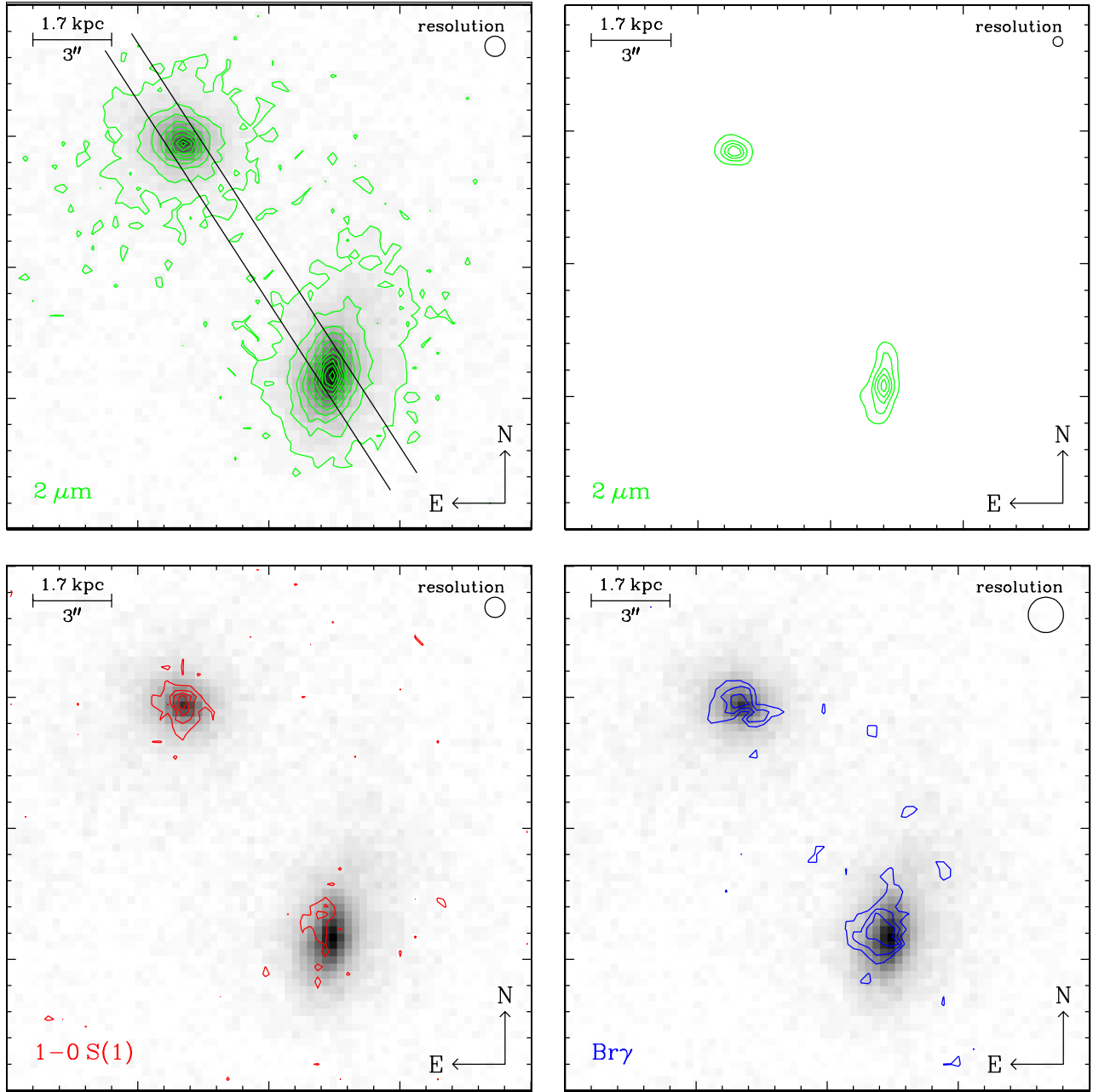


Fig. 1.— Contour maps of the $20''$ region around Mkn 266. Upper left: $2\ \mu\text{m}$ continuum. Contours are from $2\sigma\ \text{pixel}^{-1}$ at intervals of $6\sigma\ \text{pixel}^{-1}$, where $1\sigma\ \text{pixel}^{-1} \equiv 0.072\ \text{mJy arcsec}^{-2}$. Upper right: $2\ \mu\text{m}$ continuum after rebinning and deconvolving with 30 iterations of the Lucy algorithm (see Section 1 for details) at arbitrary linear intervals. Lower left: $1-0\ \text{S}(1)$ line superimposed on continuum greyscale. Contours are from $2.5\sigma\ \text{pixel}^{-1}$ at intervals of $2.5\sigma\ \text{pixel}^{-1}$, where $1\sigma\ \text{pixel}^{-1} \equiv 1.6 \times 10^{-19}\ \text{W m}^{-2}\ \text{arcsec}^{-2}$. Lower right: $\text{Br}\gamma$ line (smoothed using a 3×3 median filter, with little effect on the resolution) superimposed on continuum greyscale. Contours are from $2.5\sigma\ \text{pixel}^{-1}$ at intervals of $1.5\sigma\ \text{pixel}^{-1}$, where $1\sigma\ \text{pixel}^{-1} \equiv 2.1 \times 10^{-19}\ \text{W m}^{-2}\ \text{arcsec}^{-2}$.

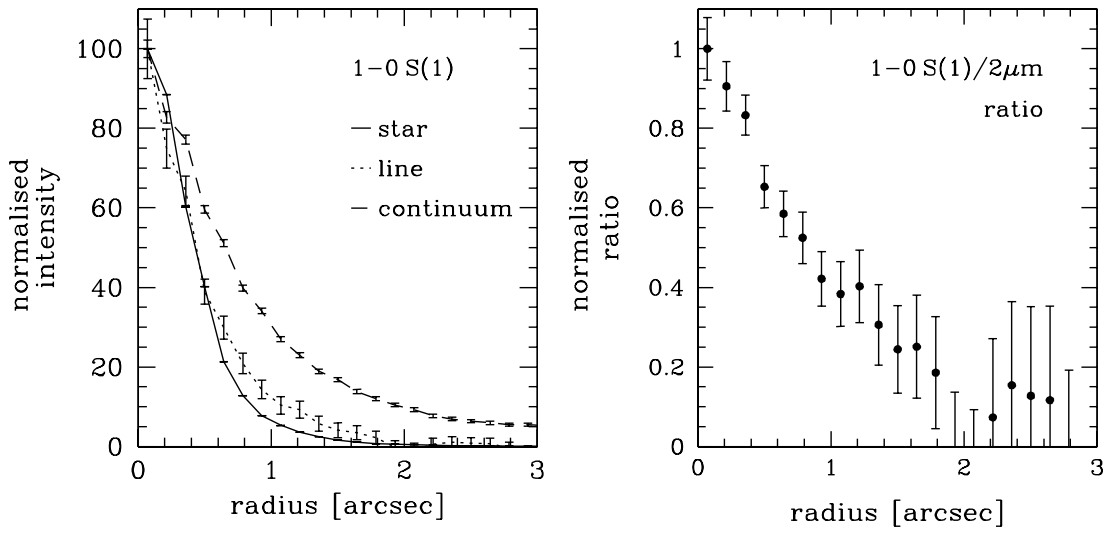


Fig. 2.— Left: Measured profiles of a star, $2\mu\text{m}$ continuum and 1-0 S(1) line in the North-East nucleus. Azimuthally averaged intensity profiles are derived from flux in concentric annuli. Right: ratio of 1-0 S(1)/ $2\mu\text{m}$ (ie normalised equivalent width of the line), decreases as a function of radius. These diagrams show clearly that the core of the 1-0 S(1) is (a) unresolved, whereas the continuum is marginally resolved; and (b) has faint wings of emission at $1-2''$.

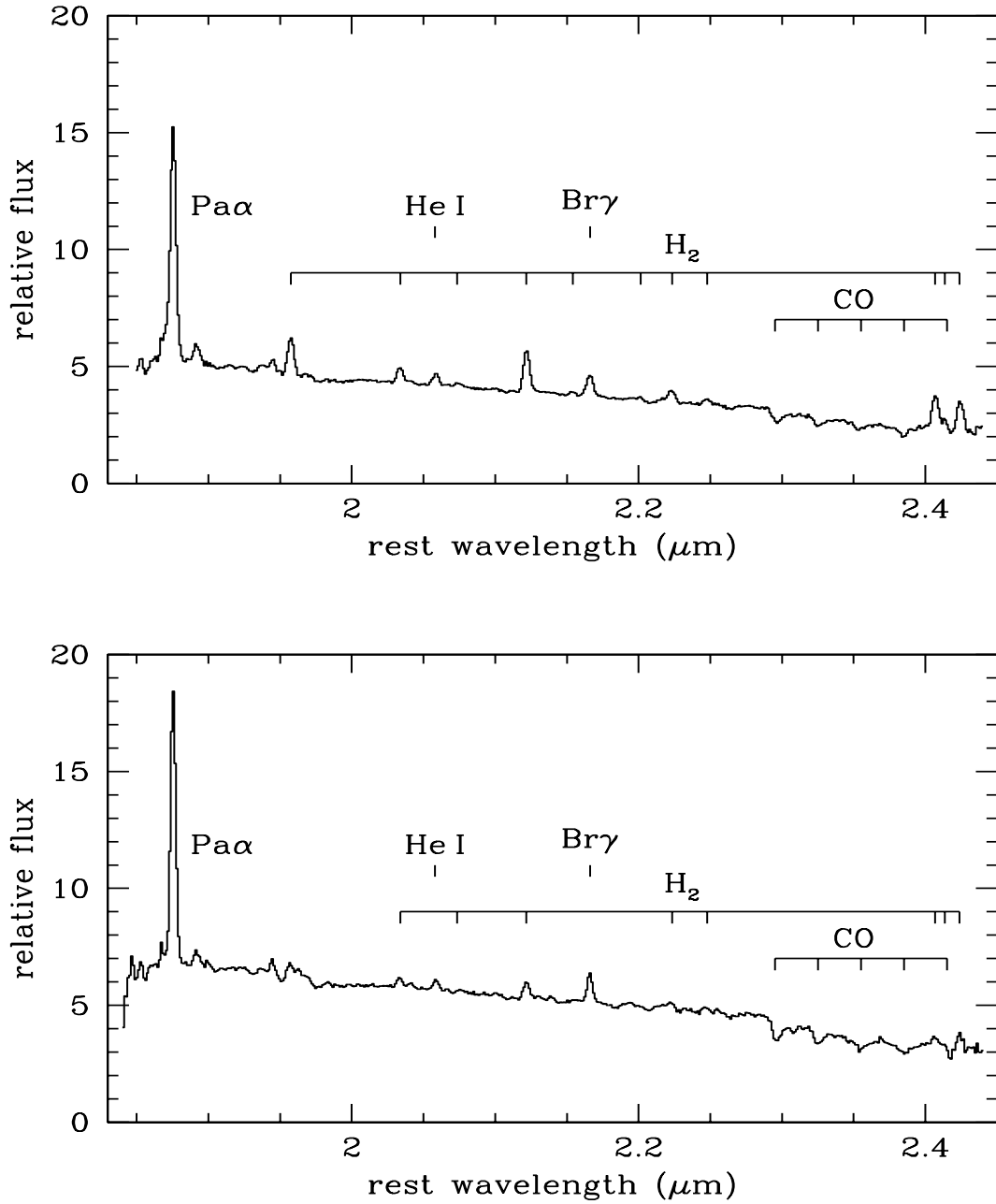


Fig. 3.— Integrated spectra of the NE (upper) and SW (lower) nuclei of Mkn 266. The important emission and absorption features are indicated. Fitting and subtraction of the continuum with stellar teplates is important in order to account for absorption features close to emission lines (eg the H₂ Q-branch).

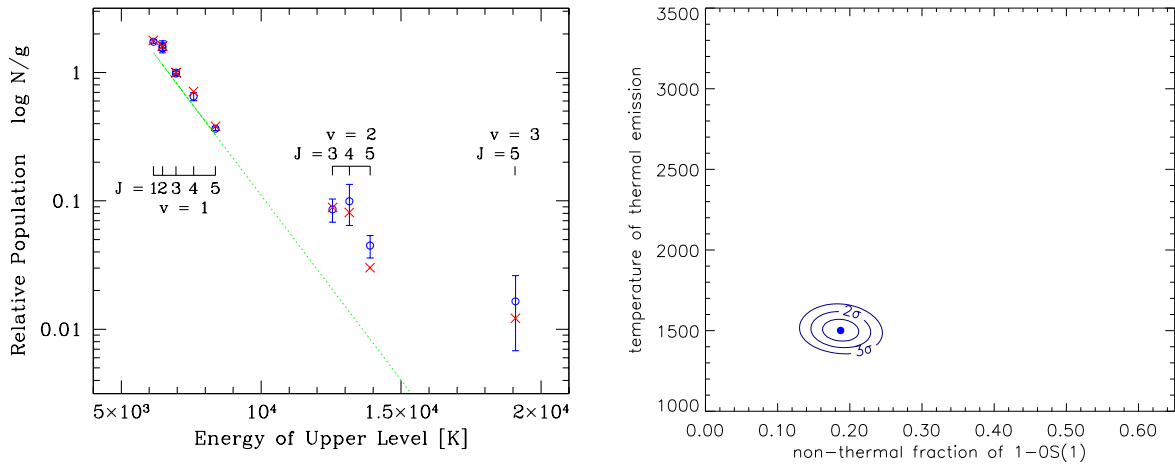


Fig. 4.— Left: Population diagram for the hot H_2 molecules in the NE nucleus, derived for 11 line transitions. The crosses denote the combined fit to the data of a thermal component (dotted line, with derived temperature $T = 1500$ K) and a non-thermal component (Black & van Dishoeck (1987) UV fluorescent model 14). The reduced chi-square $\chi^2_\nu = 0.89$, close to the expectation value $\langle 0.92 \rangle$ for 8 degrees of freedom. Right: Confidence regions for the thermal excitation temperature, T , and the non-thermal fraction of 1-0S(1), f_{UV} . The 1σ uncertainties give $T = 1500 \pm 60$ K and $f_{UV} = 0.19 \pm 0.02$ (ie fluorescent excitation accounts for 57% of the *total* H_2 line emission).

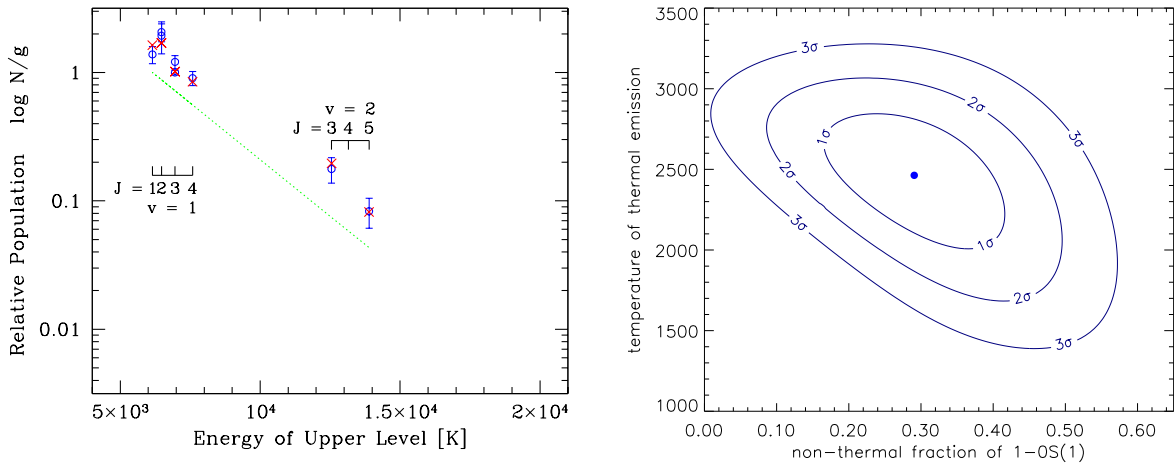


Fig. 5.— Left: Population diagram for the hot H_2 molecules in the SW nucleus, derived for 8 line transitions. The crosses denote the combined fit to the data of a thermal component (dotted line, with derived temperature $T = 2460$ K) and a non-thermal component (Black & van Dishoeck (1987) UV fluorescent model 14). The reduced chi-square $\chi^2_\nu = 1.08$, close to the expectation value $\langle 0.87 \rangle$ for 5 degrees of freedom. Right: Confidence regions for the thermal excitation temperature, T , and the non-thermal fraction of 1-0S(1), f_{UV} . The 1 σ uncertainties give $T = 2460 \pm 410$ K and $f_{UV} = 0.29 \pm 0.12$ (ie. fluorescent excitation accounts for 68% of the *total* H_2 line emission).

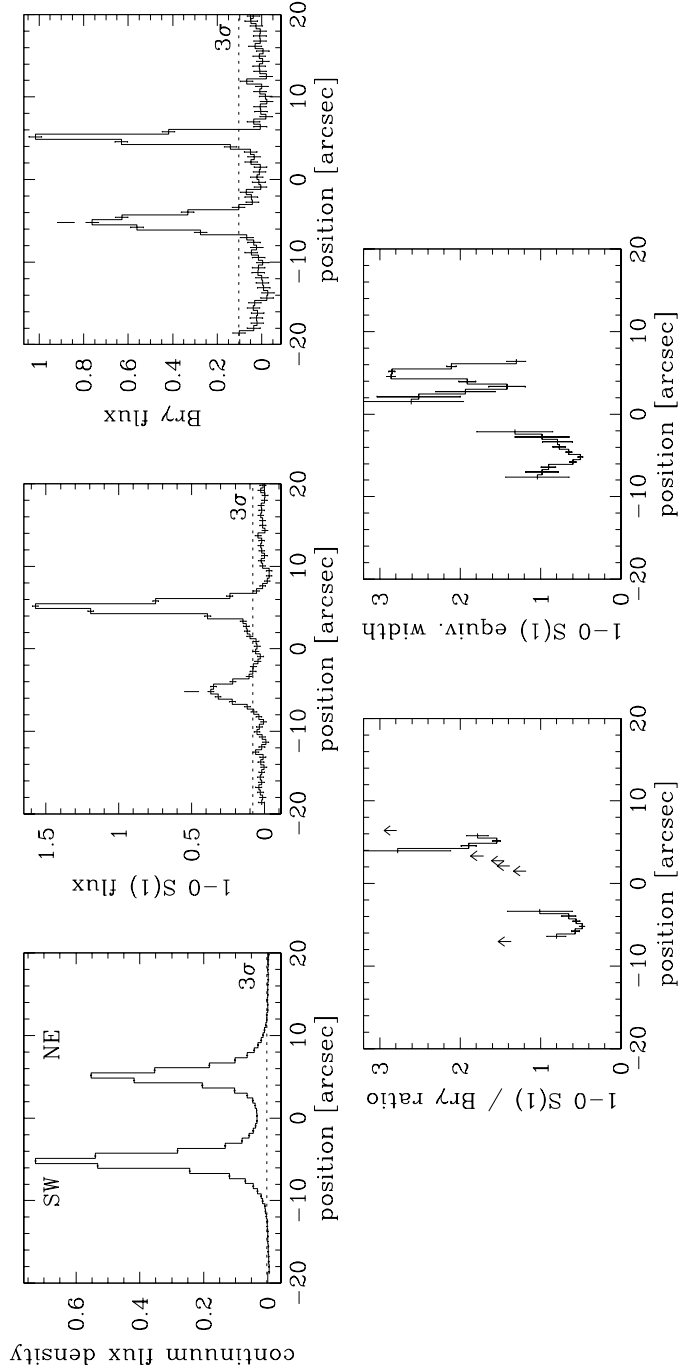


Fig. 6.— Upper: $2\mu\text{m}$ continuum, 1-0 S(1) flux, and Br γ flux, traced for $40''$ along the slit across the SW and NE nuclei. In the latter 2 figures, the vertical bar indicates the SW continuum centroid; unlike the images, no offset is seen between the 1-0 S(1) and $2\mu\text{m}$ continuum due to the poorer spatial sampling and seeing. Lower: ratio of 1-0 S(1)/Br γ and 1-0 S(1)/ $2\mu\text{m}$ (equivalent width). Away from the nuclei, both ratios increase. In the NE nucleus, the initial decrease is the same as that seen in Figure 2.